ACS OMEGA

Open Access

http://pubs.acs.org/journal/acsodf

Article

Experimental Investigation on the Pyrolysis and Conversion Characteristics of Organic-Rich Shale by Supercritical Water

Chuanjin Yao,* Fanyi Meng, Hexing Zhang, Tianyuan Di, Yiran Zhou, and Xinge Du

Cite This: *ACS Omega* 2023, 8, 49046−49056

Read Online

ACCESS | Metrics & More | Article Recommendations | Supporting Information

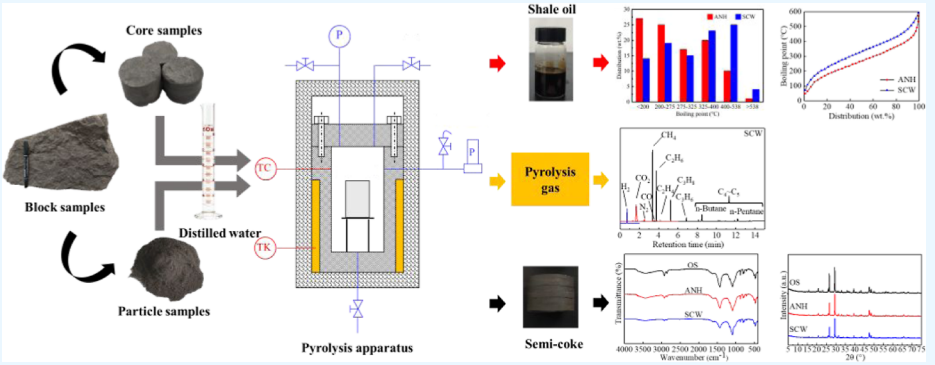

ABSTRACT: Organic-rich shale oil reservoirs with low-medium maturity have attracted increasing attention because of their enormous oil and gas potential. In this work, a series of experiments on pyrolysis of the particle and core samples were carried out in a self-made supercritical water pyrolysis apparatus to evaluate the feasibility and benefits of supercritical water in promoting the transformation efficiency and oil yield of the low-medium maturity organic-rich shale. Core samples had a mass loss of 8.4% under supercritical water pyrolysis, and many microcracks were generated, which increased the pyrolysis efficiency substantially. The oil yield of shale pyrolysis could reach 72.40% under supercritical water conditions at 23 MPa and 400 °C, which was 53.02% higher than that under anhydrous conditions. In supercritical water conditions, oxygen-containing compounds are less abundant than in anhydrous conditions, suggesting that supercritical water can inhibit their formation. Also, supercritical water conditions produced higher yields for light fraction, medium fraction, and heavy fraction shale oil than those under anhydrous conditions. These results indicate that supercritical water pyrolysis is feasible and has excellent advantages for low-medium maturity organic-rich shale.

1. INTRODUCTION

Increasing global energy demands cannot be met by conventional oil and gas resources due to rapid economic, scientific, and technological advancements. Therefore, it is very important to find out about new alternative areas for energy.[1] Shale oil and gas exploration has grown dramatically worldwide in recent years due to the tremendous success of the shale oil and gas revolution in the United States.[2−5] Currently, shale oil and gas resources have gradually developed into an alternative field to conventional oil and gas and have become increasingly important in the energy field.[6]

The low-medium organic-rich shale reservoir contains a large amount of untransformed kerogen. As reported, kerogen in the primary pores of organic-rich shale reservoirs with low-medium maturity is an immature hydrocarbon-generating medium which can produce shale oil and gas after pyrolysis. Furthermore, organic-rich shale reservoirs have the advantages of wide distribution, stability, low exploration costs, abundant resources, and easy implementation, making them a valuable unconventional oil and gas resource.[7] Despite these characteristics, it is difficult to exploit the low-medium maturity organic-rich shale resources in China due to their deep burial depth, low maturity, and poor reservoir permeability.[8,9] In situ shale conversion technology is an environmentally friendly and relatively inexpensive underground conversion mining technology that has piqued the interest of numerous research teams due to its small surface excavation, low waste emissions, and low environmental pollution. This technology involves heating shale reservoirs to transform unconverted kerogen into light hydrocarbons and natural gas products, and then lifting these products to the ground using traditional oil production technology.[6,10,11] The most widely used in situ conversion technologies for organic-rich shale reservoirs are conduction heating, radiation heating, and convection heating.[12−17]

Received: September 8, 2023
Revised: November 24, 2023
Accepted: November 29, 2023
Published: December 12, 2023

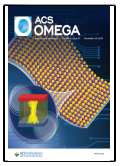

Thermal fluid convection heating is a relatively mature heating technology with advantages such as high oil and gas recovery and a fast heating speed. The advancement of near-critical and supercritical water technologies has resulted in their widespread use in the petroleum and chemical industries, including organic oil shale extraction, asphalt upgrading, coal gasification, and heavy oil upgrading.[18−21] Near-critical water (320−374 °C) and supercritical water ($T \geq 374$ °C, $P \geq 22.1$ MPa) are considered new mediums and excellent extraction solvents. Near-critical and supercritical water can dissolve hydrocarbons and participate in the reaction.[22,23] Lewan and Roy (2012)[24] conducted near-critical water extraction to extract hydrocarbons from Green River shale, Colorado, USA. It was found that shale pyrolysis at 350 °C for 72 h has a 29% higher conversion rate than anhydrous pyrolysis, indicating that water plays a significant role in hydrocarbon conversion and oil and gas formation. Ogunsola and Berkowitz (1995)[25] investigated the impact of extraction temperature and extraction time on the asphalt extraction rate of Timahdit shale and found that under optimal extraction conditions, nearly 70% of organic matter in the shale can be transformed by near-critical water. However, due to the low temperature of near-critical water, it must take a long time to obtain a high conversion rate of shale organic matter, which makes efficient conversion of shale organic matter difficult. Furthermore, hydrocarbons are more easily soluble in supercritical water than in near-critical water. Yanik (1995)[26] et al. used supercritical water to pyrolyze shale, and the results showed that compared with the anhydrous conditions (ANH) of shale, supercritical water pyrolysis had a higher yield and produced a higher content of oil properties and polar products. Olukcu (1999)[27] et al. used supercritical water and supercritical toluene to extract Beypazari shale in Turkey and found that, compared with supercritical toluene, the conversion rate of kerogen in supercritical water was higher, and the organic matter generated by supercritical water pyrolysis contained more asphaltenes and polar compounds. Funazukuri et al. (1988)[28] compared the supercritical toluene extraction, supercritical water extraction, and THF extraction of Maoming shale with dry distillation. The results showed that the hydrogen distribution of supercritical fluid extract was basically similar to that of ANH pyrolysis products, but the polar compounds in supercritical water were more easily decomposed, which was similar to the results of Olukcu et al. Hu et al. (1999)[29] have studied the pyrolysis of Huadian oil shale with near-critical and supercritical water and noted that supercritical water has the highest extract and gas yields. El Harfi et al. (1999)[30] conducted comparative experimental studies on three pyrolysis conditions of Timahdit oil shale: near-critical water, supercritical water, and ANH. Under supercritical water conditions, it was confirmed that the content of aromatics and paraffin in pyrolysis products increased and asphaltene organic matter decreased with the increase of temperature. The properties of supercritical water include a low density, low viscosity, low dielectric constant, high ion product constant, and high diffusion coefficient. Supercritical water can dissolve all types of organic matter when used as the pyrolysis medium in shale reservoirs, facilitating acid−base catalytic reactions to produce hydrocarbons from organic matter, enhancing the degree of transformation of organic matter, and improving the transformation efficiency. Furthermore, organic matter pyrolysis and uneven thermal expansion form pores and cracks in shale during supercritical water pyrolysis. The formation of pores and cracks is conducive to the migration and release of pyrolysis products. Hence, supercritical water convection heating is regarded as an effective method for the extraction of organic matter from shale. However, most studies on the pyrolysis of shale have focused on particle samples. Little is known about the pyrolysis conversion characteristics of the core samples in supercritical water. It is evident that particle samples are not pyrolyzed as in situ samples due to the absence of their original bedding structures. Consequently, guiding the in situ transformation of organic-rich shale based on particle shale samples is not rigorous. The heat and mass transfer processes inside the shale reservoir are considered in the core sample, which can more accurately simulate the pyrolysis process of underground shale than that of the particle sample.

In this work, a supercritical water pyrolysis apparatus with high temperature and high pressure (HTHP) was designed. Then, the mass loss of particle samples and core samples under supercritical water and ANH was compared, and the pyrolysis products of core samples under supercritical water and ANH were studied systematically. In addition, the effect of pyrolysis time on shale core pyrolysis transformation was also evaluated under supercritical water and ANH. The pyrolysis and transformation characteristics of shale in supercritical water were clarified. Thus, this research aims to propose an efficient pyrolysis conversion method for supercritical water for low-medium maturity organic-rich shale reservoirs and demonstrate the viability of this method so as to solve the problem of low pyrolysis efficiency for low-medium maturity shale reservoirs.

2. METHODOLOGY

2.1. Materials and Apparatus. *2.1.1. Shale Samples Preparation.* The shale core samples adopted in the experiments were from the Liangjia stop in Longkou City, China. There is an irregular, massive grayish-brown appearance in the shale samples. Table 1 presents the Fisher assay and total organic carbon TOC of the Longkou organic-rich shale samples. The shale samples prepared for the experiments are shown in Figure 1. In addition, the TOC of shale is 20.63%, which has a high conversion potential. Core samples measuring 2.5 cm in diameter and 2−3 cm in length were drilled from block samples by using a coring machine. Besides, the block samples were crushed by a solid grinder and then ground with an agate mortar to obtain particle samples with particle sizes between 60 and 100 mesh.

Table 1. Fisher Assay and TOC of Longkou Shale Samples (wt %)

components	water	residue	shale oil	gas	TOC
content	11.24	69.10	13.34	6.32	20.63

(a) Block samples (b) Core samples (c) Particle samples

Figure 1. Longkou shale sample preparation.

https://doi.org/10.1021/acsomega.3c06654
ACS Omega 2023, 8, 49046−49056

2.1.2. Supercritical Water Pyrolysis Apparatus. The experimental device is the TCWYF-1-type HTHP pyrolysis simulation experimental device of supercritical water developed by the laboratory, as shown in Figure 2.[31] The maximum

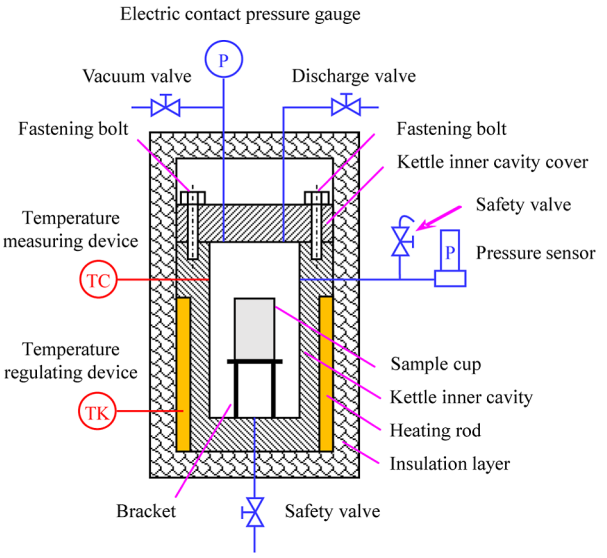

Figure 2. Self-made supercritical water pyrolysis apparatus.

working temperature is 600 °C, and the maximum working pressure is 30 MPa, which can realize the conditions of supercritical water pyrolysis ($T \geq 374$ °C, $P \geq 22.1$ MPa). The experimental device also has the properties of HTHP and corrosion resistance, which can realize the pyrolysis of shale under various temperature and pressure conditions.

The experimental device consists of a pyrolysis reaction system, a temperature control system, and a product expulsion system. The pyrolysis reaction system is the place of shale pyrolysis. The temperature control system controls the temperature process of the reactor through the computer program, transmits the real-time temperature and pressure data to the display screen, and records it through the temperature sensor and pressure sensor. The product discharge system controls the discharge of the pyrolysis products through valves.

2.2. Experimental Procedure. Different pyrolysis conditions were set at 400 °C, including ANH and low-pressure steam without adding distilled water; adding 25 mL of distilled water produces about 6 MPa pressure; under medium-pressure steam conditions, adding 50 mL of distilled water produces about 14 MPa pressure; and in supercritical water conditions, adding 100 mL of distilled water produces a pressure of 23 MPa. The experimental temperature, pressure, and water density ρ were obtained from the database of "thermophysical properties of fluid system".

The experimental procedure for shale pyrolysis is presented in Figure 3. The inner wall of the reactor and the sample cup were cleaned and dried, and a certain amount of sample was put into the sample cup; the required distilled water was calculated according to the temperature and water density and then added to the reactor chamber, covered with the kettle cover; the air in the reactor was replaced with nitrogen, its tightness was checked, and it was then vacuumed to eliminate the influence of nitrogen, carbon dioxide, oxygen, and other gases on the experiment; the reactor was connected to the computer, and the temperature and pressure data were collected from the reactor in real time; The reactor heating switch was opened, the reactor was quickly heated to 400 °C and kept at constant temperature for 2 h; stop heating when the reactor is heated to a predetermined heating time; then slowly open the reactor collecting valve to collect oil and gas products; after the pyrolysis products were collected, the product collection valve was closed; at the end of the pyrolysis experiment, the reactor was cooled rapidly to room temperature, and the shale semicoke in the reactor was removed and then sealed and dried.

Different pyrolysis conditions were set at 400 °C using the supercritical water pyrolysis apparatus, including ANH, low-pressure steam conditions (LPS), medium-pressure steam conditions (MPS), and supercritical water conditions (SCW). Table 2 shows the volume of distilled water and the pressure changes of the closed system under different pyrolysis conditions.

Table 2. Volume of Distilled Water and the Pressure Changes of the Closed System under Different Pyrolysis Conditions

Conditions	distilled water (mL)	pressure (MPa)
ANH	0	0.6−1.7
LPS	25	6.1−7.4
MPS	50	14.0−15.7
SCW	100	23.0−24.7

2.3. Product Analysis. The mass loss of shale pyrolysis was used as an evaluation index to determine the conversion effects of shale samples. Mass loss was calculated by the following equation

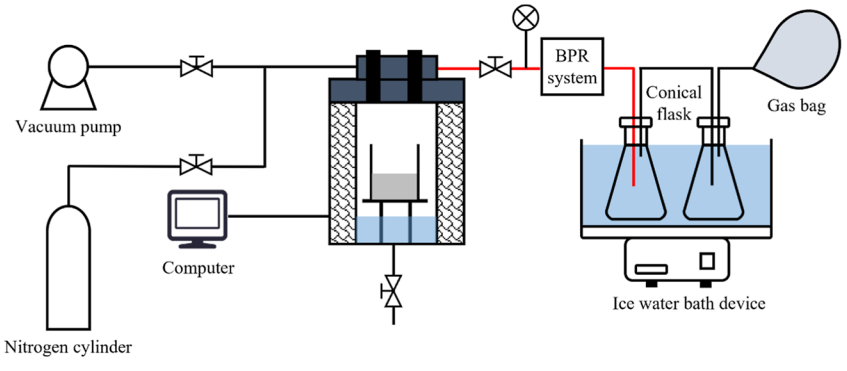

Figure 3. Experimental Procedure of shale pyrolysis.

https://doi.org/10.1021/acsomega.3c06654
ACS Omega 2023, 8, 49046−49056

$$R = \frac{m_0 - m_1}{m_0} \times 100\% \quad (1)$$

where R is the mass loss,%, m_0 is the mass of the shale sample before pyrolysis, g, and m_1 is the mass of semicoke after pyrolysis, g.

The oil yield and gas yield of shale pyrolysis were used as evaluation indexes to determine the oil and gas production capacities of the shale samples. Oil yield and gas yield are expressed as follows

$$S_o = \frac{m_o}{m_0 \cdot T_a} \times 100\% \quad (2)$$

$$S_g = \frac{m_g}{m_0 \cdot T_b} \times 100\% \quad (3)$$

where S_0 is the oil yield,%, S_g is the gas yield,%, m_0 is the mass of shale oil, g, m_g is the mass of pyrolysis gas, g, T_a is the oil content of the original shale sample,%, and T_b is the gas content of the original shale sample,%.

The Trace_1300GC-ISQ_LT temperament chromatography−mass spectrometry produced by Thermo Fisher was used to analyze the composition of the shale oil samples. The experimental procedure is as follows: a certain amount of methylene chloride was added to the shale oil sample for dissolution and transferred out of the sample bottle, and then gas chromatography−mass spectrometry analysis was carried out. The experimental conditions are as follows: The column model was TG-5, the column size was 30 m × 0.25 mm × 0.25 μm, the EI source bombardment voltage was 70 eV, the injector temperature was 300 °C, the ion source temperature was 200 °C, the line temperature was 250 °C, the carrier gas type was high purity helium, the flow rate was 0.8 mL/min, and the split ratio was 50:1. The heating procedure of the cylinder is as follows: first, it is kept at 60 °C for 5 min and then heated to 300 °C at a heating rate of 20 °C/min for 30 min.

Thermogravimetric (TG) was conducted by an STA449C synchronous thermal analyzer from Nexe, Germany. Weighing the experimental sample to 0.1 mg was accurate for a sample size of 10 mg. The heating rate was set at 10 °C/min, and the final pyrolysis temperature was 800 °C. The original shale and semicoke of shale were determined by a Nicolet iS10 Fourier transform infrared spectrometer from Thermo Scientific.

Fourier infrared spectrometer (FTIR) measurements were recorded in the luminous flux 15,000 and the region of 4000−400 cm^{-1} with a resolution of 4 cm^{-1}.[32] The samples for infrared analysis were made of about 1 mg of original shale or semicoke and 100 mg of potassium bromide, mixed and ground in an agate mortar. The mixture of the samples and potassium bromide was pressed into thin slices under 15 MPa pressure and kept for 2 min; then the infrared spectrum must then be tested immediately to avoid water absorption.

The X-ray diffraction (XRD) patterns of the original shale and semicoke were examined by the D8 ADVANCE X-ray diffractometer of Brock AXS, Germany. The experimental conditions were as follows: scanning angle 2θ was 5−75°, scanning rate was 4°/min, step length was 0.02°, tube voltage was 40 kV, and tube current was 100 mA. The spectrogram was analyzed by Jade 6.0 software.

3. RESULTS AND DISCUSSION

3.1. Effect of Sample Size on Shale Pyrolysis Transformation. As experimental samples, shale particles and shale cores were chosen, with the particle samples naturally stacked in the sample cup and the core samples manually stacked in the sample cup. A series of pyrolysis experiments were conducted to study the difference of mass loss between particle and core samples under anhydrous and supercritical water conditions at 400 °C for 3 h. The mass loss of particle samples and core samples is depicted in Figure 4.

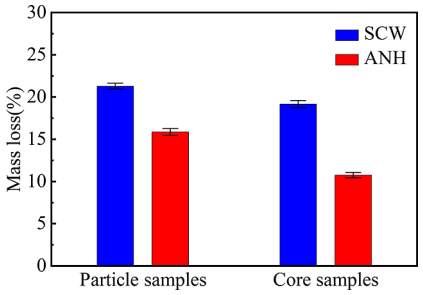

Figure 4. Effect of sample size on mass loss of the shale sample.

Compared with ANH, supercritical water conditions result in a little higher mass loss for particle samples. There is little difference in mass loss between the surface and the center of the particle samples since there is almost no temperature differential between them. However, it is observed that the mass loss of core samples under supercritical water conditions is remarkably higher than that under ANH. The mass loss of core samples in anhydrous pyrolysis is only 10.76%, while that in supercritical water reaches 19.16%, increasing by 8.4%. This increase can be attributed to the superior heat and mass transfer performance of water under supercritical conditions. On the contrary, the pyrolysis products under ANH are trapped inside the cores and eventually transformed into coke, resulting in lower mass loss. The above findings note that supercritical water still has an excellent pyrolysis effect on the internal organic matter, even for core samples. Particularly, the core samples do not destroy the structure of the shale samples, and factors such as internal heat and mass transfer rate are considered in the experiments.[33,34] In general, core samples are more accurate than particle samples in simulating underground shale pyrolysis.

3.2. Effect of Pyrolysis Conditions on Shale Pyrolysis Transformation. Figure 5 shows the effect of pyrolysis conditions on the mass loss and oil yield of core samples. The mass loss and oil yield of ANH are the lowest, which are 10.76

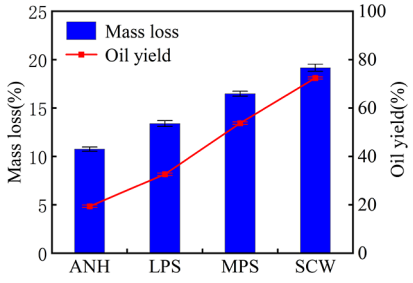

Figure 5. Effect of the pyrolysis conditions on mass loss and oil yield of core samples.

https://doi.org/10.1021/acsomega.3c06654
ACS Omega 2023, 8, 49046−49056

and 19.38%, respectively. In contrast, the mass loss and oil yield are the highest in supercritical water, which are 19.16 and 72.40%, respectively. The mass loss and oil yield of low-pressure steam and medium-pressure steam conditions are between ANH and supercritical water conditions. Shale oil and semicoke under different pyrolysis conditions are presented in Figure 6. The semicoke indicates that the core samples of

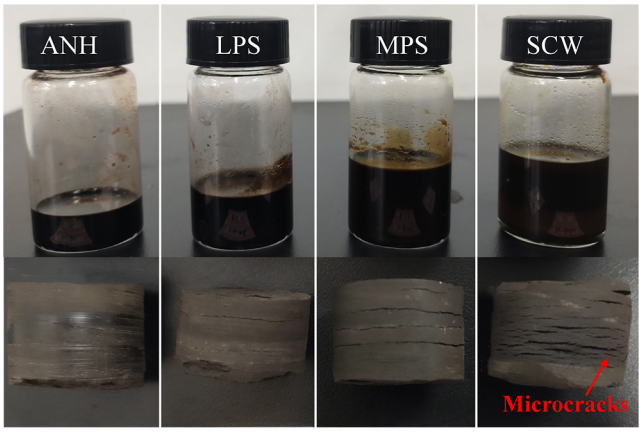

Figure 6. Shale oil and semicoke under different pyrolysis conditions.

ANH are not easy to crack. The core samples of low-pressure steam and medium-pressure steam conditions crack along the bedding direction, and the number of cracks under medium-pressure steam conditions is obviously more than that under low-pressure steam conditions. The number of cracks produced under supercritical water conditions is the largest and contains a large number of microcracks.

Compared with other pyrolysis conditions, the pyrolysis of shale in supercritical water has the highest mass loss and oil yield. The reasons are as follows: (1) the fluidity and diffusion of supercritical water make it easy for it to penetrate into the core along the bedding plane, resulting in the pyrolysis of organic matter as well as the formation of microcracks; (2) the microcracks assist supercritical water in entering shale and in releasing pyrolysis oil and gas products, contributing to organic matter's pyrolysis transformation. As a result, supercritical water has an advantage in significantly improving the pyrolysis and conversion of shale. The results of this study are consistent with those of Whitelaw et al. (2010).[35] Whitelaw et al. believe that high-pressure water is conducive to the production of oil during rock pyrolysis.

3.3. Effect of Pyrolysis Time on Shale Pyrolysis Transformation. The relationship between the mass loss and pyrolysis time of shale at 400 °C under anhydrous and supercritical water conditions is illustrated in Figure 7. With the increase of pyrolysis time, the mass loss of shale grows, but the change rate slows down gradually, indicating that prolonging pyrolysis time is conducive to the pyrolysis transformation. The mass loss of shale reaches 19.16% after pyrolysis for 3 h in supercritical water. When the pyrolysis time is increased to 5 h, the mass loss is enhanced by 0.15%. Therefore, shale treated with supercritical water at 400 °C for 3 h can be considered to have been pyrolyzed completely. On the contrary, it takes longer for shale pyrolysis to be complete under ANH. Even after 24 h of pyrolysis, the mass loss of shale is only 17.3%. In anhydrous pyrolysis, heat is transferred from the surface to the interior of the shale over a long period of

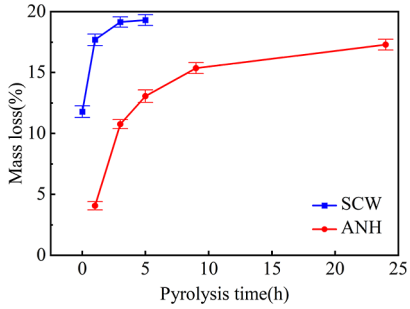

Figure 7. Effect of the pyrolysis time on the mass loss of core samples.

time. Meanwhile, shale is difficult to crack under ANH, which is unfavorable for organic matter pyrolysis and allows products to escape, resulting in shale's poor pyrolysis effect. Shale is pyrolyzed by thermal convection in supercritical water, and a large number of microcracks are formed, providing a good pathway for pyrolysis and pyrolysis products to escape. Therefore, supercritical water pyrolysis of shale can obtain a higher mass loss in a shorter pyrolysis time, which can significantly improve the pyrolysis efficiency of shale.

3.4. Characterization of Pyrolysis Gas. Gas chromatography and simulated distillation were used to test the pyrolysis gas and shale oil under anhydrous and supercritical water conditions at 400 °C for 3 h so as to clarify the properties and characteristics of oil and gas products.

Chromatographic analysis of pyrolysis gas under anhydrous and supercritical water conditions is shown in Figure 8. As part of the pyrolysis gas, there are hydrocarbon gases and nonhydrocarbon gases. Hydrocarbon gases include methane (CH_4) and heavy hydrocarbon gases (C2−C5), while nonhydrocarbon gases include CO_2 and a small amount of CO, N_2, and H_2. There is no significant difference in the hydrocarbon gas relative content, only 1.93%, while the nonhydrocarbon gas content is different, indicating that the composition of hydrocarbon gas is less affected by supercritical water. In the process of shale pyrolysis, CH_4 is mainly generated by side chain fracture of the kerogen structure, secondary reaction of shale oil at high temperature, and pyrolysis of macromolecular hydrocarbons. In fact, the fundamental source is the formation of methyl functional groups through the fracture of aromatic side chains and fat chains. The hydrocarbon gases of C2 and C3 are mainly derived from the aliphatic hydrocarbons in the free state and are formed by free radical cracking and macromolecular adipose side chain shedding, while a small amount of C4 and C5 gases are mainly formed by macromolecular structure cracking. So, no matter if the shale pyrolysis conversion is performed in supercritical water or ANH, the hydrocarbon gas composition is basically the same, and their relative volume percentage is not much different as well. Table 3 shows that more N_2 was produced in the pyrolysis gas under supercritical water conditions than under ANH. During supercritical water, complex kerogen molecules gradually open to form molecular fragments and then gradually oxidize to form small molecules. In this process, the N element in kerogen is oxidized to form N_2.[36] In addition, according to Table 3, the average molecular weight of pyrolysis gas can be calculated from the weighted average. It is found that the average molecular weight of pyrolysis gas is 33.821 in ANH and 35.509 in supercritical water conditions. It demonstrated that the average molecular weight of pyrolysis gas in supercritical water is higher.

https://doi.org/10.1021/acsomega.3c06654
ACS Omega 2023, 8, 49046−49056

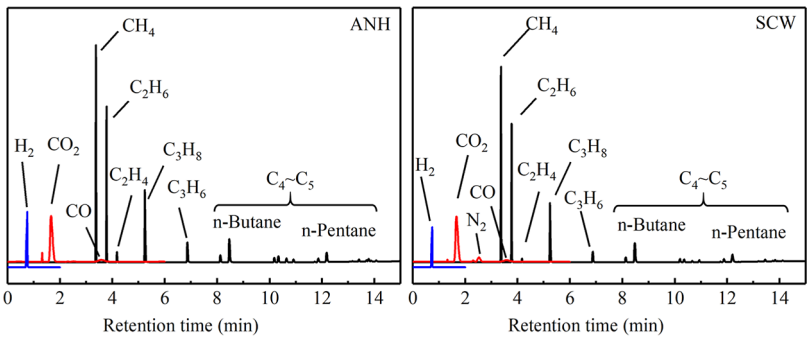

Figure 8. Chromatographic analysis of the pyrolysis gas.

Table 3. Composition of Pyrolysis Gas (vol %)

conditions	C_1	C2−C5	CO_2	CO	N_2	H_2
ANH	10.15	9.82	59.00	6.64	0.80	13.59
SCW	9.74	8.30	61.73	5.78	6.29	8.16

3.5. Characterization of Shale Oil. Shale oil generated by the pyrolysis of shale organic matter is a complex mixture. The shale oil collected under anhydrous and supercritical water conditions was analyzed by GS−MS. The contents of each component in shale oil under anhydrous and supercritical water conditions were obtained by peak area normalization of the chromatogram. The composition and distribution of shale oil are given in Supporting Information (SI) S1. The carbon number of shale oil under anhydrous and supercritical water conditions is mainly distributed between C_9−C_{31}. Under ANH, shale oil contains 75.89% aliphatic hydrocarbons, while under supercritical water conditions, aliphatic hydrocarbons are 76.95%, slightly higher than under ANH. It is also found that the content of aromatic hydrocarbons under ANH is 8.55%, while the content of aromatics under supercritical water is 12.20%. The content of aromatics in supercritical water conditions is significantly higher than that in ANH. Saturated hydrocarbons and aromatic hydrocarbons are the better-quality parts of shale oil. Saturated hydrocarbons can be used as fuels, such as straight-run gasoline, and aromatic hydrocarbons can also be used as basic raw materials for refining petrochemical products.

In addition, shale oil contains important material compositions, such as alcohol, ketone, ether, acid, and other oxygen compounds. Because of the presence of these compounds, shale oil requires secondary hydrogenation after extraction. Compared with the anhydrous condition, the oxygen-containing compound content under supercritical water conditions is lower, which indicates that supercritical water can inhibit the generation of oxygen-containing compounds during shale pyrolysis and improve the economy of in situ shale oil exploitation to a certain extent.

Figure 9 depicts the boiling point (BP) distribution and fractions of shale oil to identify the distillate of shale oil and evaluate its potential use. Shale oil with complex components produced by shale pyrolysis can be divided into six categories according to the classification standard of the distillation process in petroleum refining.[37] Naphtha (0 °C < BP < 200 °C), kerosene (200 °C < BP < 275 °C), gas oil (275 °C < BP < 325 °C), heavy gas oil (325 °C < BP < 400 °C), vacuum gas oil (400 °C < BP < 538 °C), and resin (BP > 538 °C). The classification results of shale oil fractions indicate that shale oil produced under supercritical water conditions has more extensive applications in energy and industrial fields. It can be observed from Figure 9 that the relative contents of heavy gas oil, vacuum gas oil, and residue in shale oil collected under supercritical water conditions are relatively high, especially the relative content of vacuum gas oil under supercritical water conditions. The relative content of vacuum gas oil in shale oil collected under ANH is 10%, while the relative content of vacuum gas oil in shale oil collected under supercritical water is up to 25%, which is significantly higher than that under ANH. According to the simulated distillation results of shale oil in Table 4, shale oil can be divided into three types, namely, light

Table 4. Simulated Distillation Results of Shale Oil

		components (wt %)		
conditions	initial boiling point (°C)	light fraction	medium fraction	heavy fraction
ANH	40.6	27	50	23
SCW	56.4	15	41	44

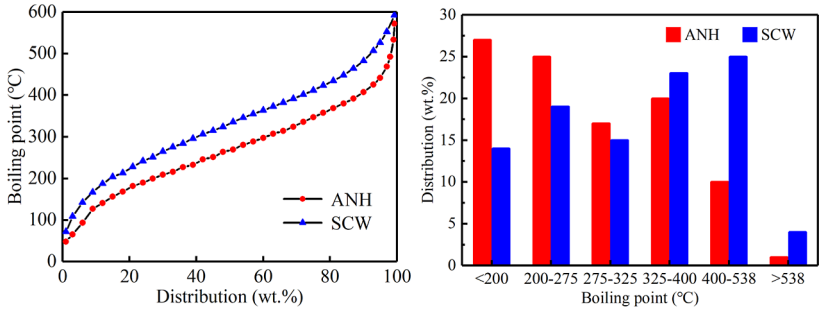

Figure 9. Boiling point distribution and fractions of shale oil.

https://doi.org/10.1021/acsomega.3c06654
ACS Omega 2023, 8, 49046−49056

fraction (BP < 200 °C), medium fraction (200 °C < BP < 350 °C), and heavy fraction (BP > 350 °C). It can be seen from Table 4 and Figure 9 that the initial boiling point of shale oil under supercritical water conditions is significantly higher than that under ANH, and the content of light and medium fractions is low, while that of the heavy fraction is high. The oil quality of shale oil in supercritical water pyrolysis is heavy, and its heavy fraction content is 21%, which is higher than that in anhydrous pyrolysis. According to the bond-breaking mechanism of organic matter pyrolysis, it can be seen that during shale organic matter pyrolysis, some molecular bonds with weak bond energy break first, but some organic matter still exists in macromolecular structures with high boiling points. These macromolecules are not volatile enough to escape spontaneously from the shale cores. Due to the solvation of supercritical water, the relatively heavy components produced by shale pyrolysis can be partially dissolved in supercritical water, miscible, and then extracted from the cores. However, heavy components with higher boiling points cannot spontaneously escape from the core under ANH, resulting in a higher relative content of light components.

The above results demonstrate that the oil and gas yield of shale obtained by supercritical water pyrolysis is higher than that obtained by anhydrous pyrolysis, but the fraction of shale oil is heavier, and the average molecular weight of the pyrolysis gas is higher.

3.6. Yield of Pyrolysis Oil and Gas Products. Since only oil and gas products were evaluated by analyzing the composition of shale oil and gas, it is necessary to calculate the mass of each component of pyrolysis oil and gas products based on the yield. The mass of shale oil collected under anhydrous and supercritical water conditions is 2.56 and 9.47 g, and the oil yield is 19.38 and 72.40%, respectively. The oil yield in supercritical water pyrolysis is 53.02% higher than that in anhydrous pyrolysis. According to the simulated distillation results of shale oil in Table 4, the mass of each component of shale oil was calculated, as shown in Table 5. The mass of pyrolysis gas collected under anhydrous and supercritical water conditions is 0.26 and 1.11 g, and the gas yield is 4.15 and 17.91%, respectively. The gas yield in supercritical water pyrolysis is 13.76%, which is higher than that in anhydrous pyrolysis. According to the gas chromatographic results of pyrolysis gas in Table 3, the gas mass fraction was obtained from the gas volume fraction, and then the mass of each component of pyrolysis gas was calculated, as shown in Table 6.

Table 5. Mass of Each Component of Shale Oil

conditions	light fraction (g)	medium fraction (g)	heavy fraction (g)	total mass (g)
ANH	0.69	1.28	0.59	2.56
SCW	1.42	3.88	4.17	9.47

The yield of each component of shale oil under supercritical water conditions is higher than that under ANH, which indicates that supercritical water can extract light hydrocarbons, medium hydrocarbons, and heavy hydrocarbons. Due to the excellent solvation effect of supercritical water, the lighter components of shale oil can be transferred into the aqueous phase. Meanwhile, the relatively heavy components can be partially dissolved in supercritical water, resulting in miscibility. As a result, both the light components and the heavy components can be extracted by supercritical water.[38−40] Under supercritical water conditions, each component of the pyrolysis gas has a higher mass than that under ANH. The yield of the pyrolysis oil and gas products was used to directly evaluate the pyrolysis effect. The results show that the pyrolysis reaction of shale in supercritical water is stronger, so the oil and gas yield is higher. Furthermore, the yield of each component of shale oil and pyrolysis gas is higher under supercritical water conditions. Therefore, supercritical water pyrolysis has significant advantages for low-medium maturity organic-rich shale.

3.7. Characterization of Semicokes. The FTIR, TG, and XRD analyses were conducted on the original shale (OS) and the semicoke collected from the pyrolysis of shale cores under anhydrous and supercritical water conditions at 400 °C for 3 h to further evaluate the effect of the supercritical water on low-medium maturity organic-rich shale pyrolysis transformation.

3.7.1. FTIR Analysis. The aliphatic hydrocarbon structure closely affects the hydrocarbon generation characteristics of shale pyrolysis. Volatiles are mainly generated from aliphatic hydrocarbons in organic shale organic matter. Hence, the hydrocarbon generation characteristics of shale pyrolysis are analyzed based on the aliphatic hydrocarbon structure.[41] Figure 10 shows the FTIR diagrams of the original shale and semicoke. By analyzing the results of FTIR, a significant change in the absorption peaks of organic functional groups can be inferred after pyrolysis. The absorption peaks at 2920 and 2850 cm^{-1} belong to the absorption peaks of aliphatic C−H functional groups, and their intensity decreases significantly.[42] The infrared quantitative analysis method adopted the external standard method. The microcrystalline paraffin containing 100% aliphatic chains was used as the standard sample, and the peak area of the characteristic peak at 3000−2800 cm^{-1} was calculated to analyze the relative content of aliphatic hydrocarbons in the original shale and semicoke. The aliphatic hydrocarbon content of the original shale is 22.60%,

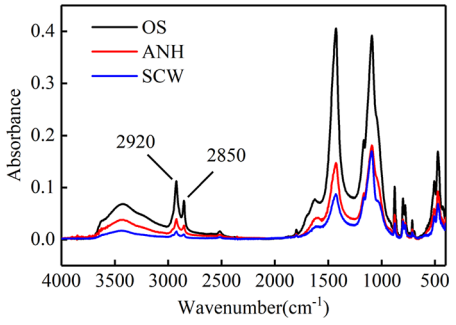

Figure 10. FTIR diagrams of original shale and semicoke.

Table 6. Mass of Each Component of Pyrolysis Gas

conditions	C_1 (g)	C_2−C_5 (g)	CO_2 (g)	CO (g)	N_2 (g)	H_2 (g)	total mass (g)
ANH	0.012	0.030	0.200	0.014	0.002	0.002	0.26
SCW	0.049	0.101	0.849	0.051	0.055	0.005	1.11

https://doi.org/10.1021/acsomega.3c06654
ACS Omega 2023, 8, 49046−49056

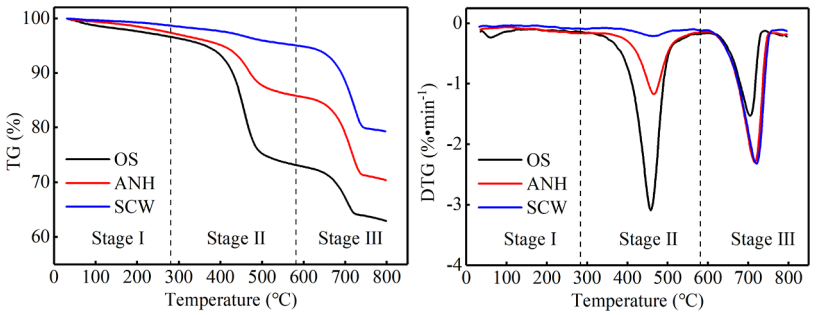

Figure 11. TG-DTG curves of original shale and semicokes.

Table 7. Pyrolysis Characteristics Parameter Analysis of Various Stages of Original Shale and Semi-Cokes

	stage I			stage II		stage III			
conditions	interval/°C	TG/%	interval /°C	T_{max}/°C	TG/%	interval /°C	T_{max}/°C	TG/%	total mass loss/%
OS	<280	3.38	280−590	458	25.60	590−800	705	8.07	37.05
ANH	<280	2.63	280−590	465	11.66	590−800	716	15.30	29.59
SCW	<280	1.33	280−590	464	3.71	590−800	720	15.61	20.65

and the aliphatic hydrocarbon content of semicoke under anhydrous and supercritical water conditions is 9.03 and 3.51%, respectively, indicating that the pyrolysis transformation of organic matter is more sufficient under supercritical conditions.

3.7.2. TG Analysis. As described in Figure 11, the TG-DTG curves of the original shale and semicoke in the nitrogen atmosphere. Shale pyrolysis can be divided into three stages based on the TG curves of the original shale.[43] The temperature range of the first stage is less than 280 °C, which is the precipitation of crystalline water. The second stage is the decomposition of organic matter at 280−590 °C. The third stage is the decomposition of minerals in the temperature range of 590−800 °C. TG results showed that the original shale and the semicoke under ANH have two weightlessness periods in stage II and stage III, respectively. However, the semicoke of supercritical water pyrolysis is not evident in stage II. According to the comparative analysis of DTG results, there are two evident peaks of the original shale and the semicoke under ANH in stage II and stage III, respectively, while the peak of the semicoke of stage II under supercritical water conditions is not obvious.

According to the FTIR analysis of shale semicoke in Figure 11, the semicoke contains organics that are not fully pyrolyzed. Therefore, TG analysis of shale semicoke can further illustrate the degree of pyrolysis of organic matter in semicoke. According to Table 7, in stages I and II, the total mass loss of the semicoke under ANH is 14.3%, under supercritical water conditions is 5.06%, and the total mass loss of the semicoke under supercritical water conditions is relatively low. Clearly, supercritical water suffices for the pyrolysis transformation of shale organic matter.

3.7.3. XRD Analysis. Figure 12 depicts the XRD patterns of the original shale and semicoke. The inorganic minerals of the original shale contain 23% quartz, 49% calcite, 6% pyrite, 6% analcime, 3% plagioclase, and 13% clay minerals (Table 8). Compared with the original shale, the inorganic minerals of the semicoke change slightly under ANH, and the clay minerals remove free water and bound water, resulting in a decrease in the relative content of clay minerals. However, the dehydration of clay minerals also occurs in semicoke of supercritical water pyrolysis. Furthermore, it is also found that the characteristic

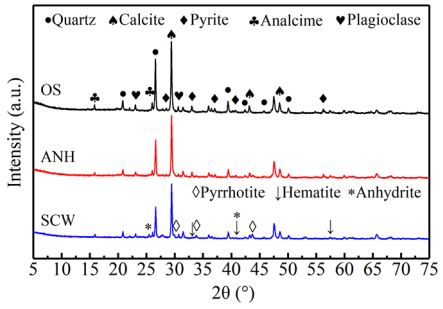

Figure 12. XRD patterns of original shale and semicoke.

peaks of pyrrhotite (FeS), hematite (Fe_2O_3), and anhydrite ($CaSO_4$) appear; these phenomena are not found in the XRD patterns of the semicoke under ANH. For the original shale, the pyrite is 6%. After supercritical water pyrolysis, the pyrite content decreases to 1%, and the pyrrhotite and hematite reach 5 and 2%, respectively, which indicates the conversion of pyrite decomposes into pyrrhotite and hematite in supercritical water. Lv et al. (2017)[44] used the following reaction to account for pyrite decomposition in H_2O or CO_2. The results indicate that supercritical water promotes the decomposition of pyrite in shale, making it easier for it to decompose. In the pyrolysis research of shale pyrite, it is pointed out that the decomposition of pyrite is beneficial to promote and accelerate the formation of free radicals in kerogen and further promotes the pyrolysis of shale to generate oil.[45,46] Therefore, the decomposition of pyrite strengthens the pyrolysis of shale organic matter, which suggests that supercritical water pyrolysis may be more advantageous for shale with a high pyrite content. In addition, calcium compounds in shale react with sulfur dioxide to form calcium sulfate in supercritical water.

$$FeS_2 \rightarrow Fe_{1-x}S + S_2 \quad (4)$$

$$FeS + CO_2 \rightarrow Fe_xO_y + SO_2 + CO \quad (5)$$

$$FeS + H_2O \rightarrow Fe_xO_y + SO_2 + H_2 \quad (6)$$

Although pyrite in Longkou shale has been decomposed, the content of pyrite is low. It can be considered that in a

https://doi.org/10.1021/acsomega.3c06654
ACS Omega 2023, 8, 49046−49056

Table 8. Mineral Composition of Domanic Rock Before and After in Anhydrous and Supercritical Waters Pyrolysis

	mineral compound (wt %)								
conditions	quartz	calcite	pyrite	analcime	plagioclase	pyrrhotite	hematite	anhydrite	clay minerals
OS	23	49	6	6	3				13
ANH	21	60	6	6	2			1	4
SCW	21	54	1	5	5	5	2	3	4

supercritical water environment at 400 °C, the mass loss of shale has little relationship with the decomposition of inorganic minerals, and the mass loss of shale is caused by the pyrolysis of organic matter.

4. CONCLUSIONS

In this article, the pyrolysis experiments of Longkou shale under anhydrous and supercritical water conditions were conducted by using a self-designed HTHP pyrolysis device. Three factors influencing shale pyrolysis have been thoroughly investigated: sample size, pyrolysis conditions, and pyrolysis time. The pyrolysis oil and gas products of the core samples were thoroughly investigated under supercritical water and ANH. The following conclusions can be drawn:

1 Core samples pyrolyze differently than particle samples, and the mass loss of core samples in supercritical water is significantly greater than in ANH. The core samples, in particular, do not destroy the shale's flake structure and can more realistically simulate the pyrolysis process of low-medium maturity organic-rich shale.

2 The higher mass loss and oil and gas yield of shale core pyrolysis are obtained in supercritical water, 19.16, 72.40, and 17.91%, respectively. Core samples produced a large number of microcracks along the bedding direction, resulting in the timely release of pyrolysis products, which markedly promoted the pyrolysis of shale. The oil yield is high when the core samples are pyrolyzed with supercritical water, but the fraction of shale oil is heavy. However, the yield of each component of shale oil under supercritical water conditions is higher than that under ANH.

3 TG and FTIR analyses indicate that the shale organic matter has been completely pyrolyzed. The XRD analysis of semicoke in supercritical water reveals that the characteristic peaks of pyrite (FeS_2) disappear, but the characteristic peaks of pyrrhotite (FeS), hematite (Fe_2O_3), and anhydrite ($CaSO_4$) appear. It has been confirmed the feasibility and superiority of low-medium maturity organic-rich shale pyrolysis in supercritical water.

■ ASSOCIATED CONTENT

Supporting Information

The Supporting Information is available free of charge at https://pubs.acs.org/doi/10.1021/acsomega.3c06654.

Composition distribution of shale oil (PDF)

■ AUTHOR INFORMATION

Corresponding Author

Chuanjin Yao − *Key Laboratory of Unconventional Oil & Gas Development (China University of Petroleum (East China)), Ministry of Education, Qingdao 266580, P. R. China; School of Petroleum Engineering and Shandong Provincial Key Laboratory of Oilfield Chemistry, China University of Petroleum (East China), Qingdao 266580, P. R. China;* orcid.org/0000-0002-6125-8991; Email: cy375@upc.edu.cn

Authors

Fanyi Meng − *Key Laboratory of Unconventional Oil & Gas Development (China University of Petroleum (East China)), Ministry of Education, Qingdao 266580, P. R. China; School of Petroleum Engineering, China University of Petroleum (East China), Qingdao 266580, P. R. China*

Hexing Zhang − *Key Laboratory of Unconventional Oil & Gas Development (China University of Petroleum (East China)), Ministry of Education, Qingdao 266580, P. R. China; School of Petroleum Engineering, China University of Petroleum (East China), Qingdao 266580, P. R. China*

Tianyuan Di − *Key Laboratory of Unconventional Oil & Gas Development (China University of Petroleum (East China)), Ministry of Education, Qingdao 266580, P. R. China; School of Petroleum Engineering, China University of Petroleum (East China), Qingdao 266580, P. R. China*

Yiran Zhou − *Key Laboratory of Unconventional Oil & Gas Development (China University of Petroleum (East China)), Ministry of Education, Qingdao 266580, P. R. China; School of Petroleum Engineering, China University of Petroleum (East China), Qingdao 266580, P. R. China*

Xinge Du − *Key Laboratory of Unconventional Oil & Gas Development (China University of Petroleum (East China)), Ministry of Education, Qingdao 266580, P. R. China; School of Petroleum Engineering, China University of Petroleum (East China), Qingdao 266580, P. R. China*

Complete contact information is available at: https://pubs.acs.org/10.1021/acsomega.3c06654

Notes

The authors declare no competing financial interest.

■ ACKNOWLEDGMENTS

This research was supported by the National Natural Science Foundation of China (grant no. 51974341 and U22B6004) and the Fundamental Research Funds for the Central Universities (no. 20CX06070A). We also appreciate the reviewers and editors for their constructive comments to make the paper of high quality.

■ REFERENCES

(1) Zou, C. N.; Zhai, G. M.; Zhang, G. Y.; Wang, H. J.; Zhang, G. S.; Li, J. Z.; Wang, Z. M.; Wen, Z. X.; Ma, F.; Liang, Y. B.; Yang, Z.; Li, X.; Liang, K. Formation, distribution, potential and prediction of global conventional and unconventional hydrocarbon resources. *Petrol. Explor. Dev.* **2015**, *42* (1), 14−28.

(2) Kilian, L. The impact of the shale oil revolution on US oil and gasoline prices. *Rev. Environ. Econ. Pol.* **2016**, *10* (2), 185−205.

(3) Jarvie, D. M. Shale resource systems for oil and gas: Part 2—Shale-oil resource systems. *Shale reservoirs—Giant resources for the*

21st century; Breyer, J. A., Ed.; AAPG Memoir, 2012; Vol. *97*, pp 89−119.
(4) Rajnauth, J. Is it time to focus on unconventional resources?. *Presented at the SPETT 2012 Energy Conference and Exhibition, Port-of-Spain, Trinidad*, 2012; SPE Paper 158654.
(5) Sarg, J. F. The Bakken-an unconventional petroleum and reservoir system. *Golden: Office of Scientific & Technical Information Technical Reports*, 2012.
(6) Zhao, W. Z.; Hu, S. Y.; Hou, L. H. Connotation and strategic role of in-situ conversion processing of shale oil underground in the onshore China. *Petrol. Explor. Dev.* **2018**, *45* (4), 563−572.
(7) Zhao, W. Z.; Hu, S. Y.; Hou, L. H.; Yang, T.; Li, X.; Guo, B.; Yang, Z. Types and resource potential of continental shale oil in China and its boundary with tight oil. *Petrol. Explor. Dev.* **2020**, *47* (1), 1−11.
(8) Zou, C. N.; Yang, Z.; Cui, J. W.; Zhu, R. K.; Hou, L. H.; Tao, S. Z.; Yuan, X. J.; Wu, S. T.; Lin, S. H.; Wang, L.; Bai, B.; Yao, J. L. Formation mechanism, geological characteristics and development strategy of nonmarine shale oil in China. *Petrol. Explor. Dev.* **2013**, *40* (1), 15−27.
(9) Yang, Z.; Hou, L. H.; Tao, S. Z.; Cui, J. W.; Wu, S. T.; Lin, S. H.; Pan, S. Formation conditions and "sweet spot" evaluation of tight oil and shale oil. *Petrol. Explor. Dev.* **2015**, *42* (5), 555−565.
(10) Wang, Y. P.; Wang, Y. W.; Meng, X. L.; Su, J. Z.; Li, F. X.; Li, Z. T. Enlightenment of American's oil shale in-situ retorting technology. *Oil Drill. Prod. Technol.* **2013**, *35* (6), 55−59.
(11) Cui, J. W.; Zhu, R. K.; Hou, L. H. Shale in-situ mining technology status quo of challenges and opportunities. *Unconv. Oil Gas* **2018**, *5* (6), 103−114.
(12) Burton, I. R. S.; Cha, C. Y.; Ridley, R. D. Apparatus for obtaining uniform gas flow through an in situ oil shale retort. U.S. Patent US3,941,421A, 1976.
(13) Bartis, J. T.; Latourrette, T.; Dixon, L.; Peterson, D. J.; Cecchine, G. *Oil Shale Development in the United States*; Prospects and policy issues: Rand Corporation, 2005.
(14) Cook, E. W. Oil-shale technology in the USA. *Fuel* **1974**, *53* (3), 146−151.
(15) Kang, Z. Q.; Zhao, Y. S.; Yang, D. Review of oil shale in-situ conversion technology. *Appl. Energy* **2020**, *269*, 115121.
(16) Dammer; Anton, R.; Killen; James, C.; Biglarbigi; Khosrow; Crawford, P.; Johnson, H. *Secure Fuels from Domestic Resources: The Continuing Evolution of America's Oil Shale and Tar Sands Industries*; United States Department of Energy; Office of Petroleum Reserves, Office of Naval and Oil Shale Reserves, 2007.
(17) Zhao, Y. S.; Feng, Z. C.; Yang, D. The method for mining oil & gas from oil shale by convection heating. CN200510012473, 2005.
(18) Feng, H. F.; Sun, J. L.; Jin, H.; Kou, J. J.; Guo, L. J. Char suppression mechanism using recycled intermediate phenol in supercritical water gasification of coal. *Fuel* **2021**, *305* (2), 121441.
(19) Al-Muntaser, A. A.; Varfolomeev, M. A.; Suwaid, M. A.; Yuan, C.; Chemodanov, A. E.; Feoktistov, D. A.; Rakhmatullin, I. Z.; Abbas, M.; Domínguez-Álvarez, E.; Akhmadiyarov, A. A.; et al. Hydrothermal upgrading of heavy oil in the presence of water at sub-critical, near-critical and supercritical conditions. *J. Petrol. Sci. Eng.* **2020**, *184*, 106592.
(20) Fedyaeva, O. N.; Antipenko, V. R.; Vostrikov, A. A. Peculiarities of composition of hydrocarbon and heteroatomic substances obtained during conversion of kashpir oil shale in supercritical water. *Russ. J. Phys. Chem. B* **2017**, *11* (8), 1246−1254.
(21) Sato, T.; Adschiri, T.; Arai, K.; Rempel, G. L.; Ng, F. T. Upgrading of asphalt with and without partial oxidation in supercritical water. *Fuel* **2003**, *82* (10), 1231−1239.
(22) Savage, P. E. Organic chemical reactions in supercritical water. *Chem. Rev.* **1999**, *99* (2), 603−622.
(23) Franck, E. U. Physicochemical properties of supercritical solvents (Invited lecture). *Ber. Bunsengesellschaft Phys. Chem.* **1984**, *88* (9), 820−825.
(24) Lewan, M. D.; Roy, S. Role of water in hydrocarbon generation from Type-I kerogen in Mahogany oil shale of the Green River Formation. *Org. Geochem.* **2011**, *42* (1), 31−41.
(25) Ogunsola, O. M.; Berkowitz, N. Extraction of oil shales with sub- and near-critical water. *Fuel Process. Technol.* **1996**, *37* (3), 185.
(26) Yanik, J.; Yüksel, M.; Sağlam, M.; Olukçu, N.; Bartle, K.; Frere, B. Characterization of the oil fractions of shale oil obtained by pyrolysis and supercritical water extraction. *Fuel* **1995**, *74* (1), 46−50.
(27) Olukcu, N.; Yanik, J.; Saglam, M.; Yuksel, M.; Karaduman, M. Solvent Effect on the Extraction of Beypazari Oil Shale. *Energy Fuel.* **1999**, *13* (4), 895−902.
(28) Funazukuri, T.; Yokoi, S.; Wakao, N. Supercritical fluid extraction of Chinese Maoming oil shale with water and toluene. *Fuel* **1988**, *67* (1), 10−14.
(29) Hu, H. Q.; Zhang, J.; Guo, S. C.; Chen, G. H. Extraction of Huadian oil shale with water in sub-and supercritical states. *Fuel* **1999**, *78* (6), 645−651.
(30) El harfi, K.; Bennouna, C.; Mokhlisse, A.; Ben chanâa, M.; Lemée, L.; Joffre, J.; Amblès, A. Supercritical fluid extraction of Moroccan (Timahdit) oil shale with water. *J. Anal. Appl. Pyrol.* **1999**, *50* (2), 163−174.
(31) Yao, C. J.; Zheng, Y.; Li, L.; Du, D. F.; Lei, G. L.; Chen, D. C. Design of simulation experimental system for high temperature and high pressure steam pyrolysis. *Exp. Technol. Manag.* **2019**, *36* (6), 104−107.
(32) Smith, A. L. *Applied Infrared Spectroscopy. Fundamentals, Techniques and Analytical Problem Solving*; Wiley, 1979.
(33) Shih, S.; Sohn, H. Y. A mathematical model for the retorting of a large block of oil shale: Effect of the internal temperature gradient. *Fuel* **1978**, *57* (10), 622−630.
(34) Gregg, M. L.; Campbell, J. H.; Taylor, J. R. Laboratory and modelling investigation of a Colorado oil-shale block heated to 900 C. *Fuel* **1981**, *60* (3), 179−188.
(35) Whitelaw, P.; Uguna, C. N.; Stevens, L. A.; Meredith, W.; Snape, C. E.; Vane, C. H.; Moss-Hayes, V.; Carr, A. D. Shale gas reserve evaluation by laboratory pyrolysis and gas holding capacity consistent with field data. *Nat. Commun.* **2019**, *10*, 3659.
(36) Vostrikov, A. A.; Shishkin, A. V.; Sokol, M. Y.; Dubov, D. Y.; Fedyaeva, O. N. Conversion of brown coal continuously supplied into the reactor as coal−water slurry in a supercritical water and water−oxygen mixture. *J. Supercrit. Fluids* **2016**, *107*, 707−714.
(37) Na, J. G.; Im, C. H.; Chung, S. H.; Lee, K. B. Effect of oil shale retorting temperature on shale oil yield and properties. *Fuel* **2012**, *95*, 131−135.
(38) Cheng, Z. M.; Ding, Y.; Zhao, L. Q.; Yuan, P. Q.; Yuan, W. K. Effects of supercritical water in vacuum residue upgrading. *Energy Fuel.* **2009**, *23* (6), 3178−3183.
(39) Canıaz, R. O.; Erkey, C. Process intensification for heavy oil upgrading using supercritical water. *Chem. Eng. Res. Des.* **2014**, *92* (10), 1845−1863.
(40) Tan, X. C.; Liu, Q. K.; Zhu, D. Q.; Yuan, P. Q.; Cheng, Z. M.; Yuan, W. K. Pyrolysis of heavy oil in the presence of supercritical water: The reaction kinetics in different phases. *AIChE J.* **2015**, *61* (3), 857−866.
(41) Wang, Q.; Xu, X. C.; Chi, M. S.; Zhang, H. X.; Bai, J. R. FT-IR study on composition of oil shale kerogen and its pyrolysis oil generation characteristics. *J. Fuel Chem. Technol.* **2015**, *43* (10), 1158.
(42) Lan, X.-Z.; Luo, W. J.; Song, Y. H.; Zhang, Q. L.; Zhou, J. Study on the spectrum research on the process of oil shale pyrolysis. *Spectrosc. Spectral Anal.* **2016**, *36* (4), 1121−1126.
(43) Kang, Z. Q. *Pyrolysis Characteristics of Oil Shale and Simulation Study of In Situ Injection Thermal Recovery of Oil and Gas*; Taiyuan University of Technology, 2008.
(44) Lv, W. Z.; Yu, D. X.; Wu, J. Q.; Yu, X.; Du, Y. F.; Yao, H.; Xu, M. H. A kinetic study on oxidation of ferrous sulfide (FeS) in mixtures of CO2 and H2O. *Proc. Combust. Inst.* **2017**, *36* (2), 2173−2180.

https://doi.org/10.1021/acsomega.3c06654
ACS Omega 2023, 8, 49046−49056

(45) Gai, R. H.; Jin, L. J.; Zhang, J. B.; Wang, J. Y.; Hu, H. Q. Effect of inherent and additional pyrite on the pyrolysis behavior of oil shale. *J. Anal. Appl. Pyrol.* **2014**, *105*, 342−347.
(46) Bakr, M. Y.; Yokono, T.; Sanada, Y.; Akiyama, M. Role of pyrite during the thermal degradation of kerogen using in situ high-temperature ESR technique. *Energy Fuel.* **1991**, *5* (3), 441−444.

https://doi.org/10.1021/acsomega.3c06654
ACS Omega 2023, 8, 49046−49056